INVESTIGATION OF SMOKE CHARACTERISTICS BY PHOTOMETRIC MEASUREMENTS

Kristian Börger[1,2], Alexander Belt[2], Alica Kandler[2], Thorsten Schultze[3], Lukas Arnold[1,2]

[1]University of Wuppertal, Wuppertal, 42119, NRW, Germany
[2]Jülich Research Center, Jülich, 52428, NRW, Germany
[3]University of Duisburg-Essen, Duisburg, 47057, NRW Germany

e-mail: boerger@uni-wuppertal.de

ABSTRACT

Visibility in case of fire can be predicted from CFD simulations as a major tenability criterion within the scope of performance-based safety concepts. Indications that light extinction might be significantly overestimated by numerical fire models [McGrattan, 2022] have been confirmed by experimental investigations and simulations [Arnold, 2021] with the Fire Dynamics Simulator (FDS). For this purpose, a novel photometric approach was applied in the context of EN 54 [EN54, 2002] test fires among established measurement methods for the determination of spatial and temporal resolved light extinction coefficients. Common DSLR cameras capture the relative change in the intensity of individual light sources (LEDs) due to fire smoke. Based on geometrical optics as well as the Beer-Lambert's law, an inverse model deduces local values of the extinction coefficient, assuming a homogeneous smoke layering. Both, the quality, and the scope of the experimental setup have been incrementally optimized and extended. Potential sources of error were examined, such as temperature-related effects on the LEDs' intensity.
Besides the spatial resolution of the smoke density, the focus of recent investigations is on the in-depth smoke characteristics. For this reason, light obscuration was assessed at multiple wavelengths. Furthermore, aging of aerosols was analyzed by measuring the change in particle size distribution at different heights of the smoke layering.
This paper introduces an innovative approach for the acquisition of reliable data to validate the prediction of smoke propagation by numerical fire models. The extensive dataset of the latest investigation covers n-heptane pool fires as well as wood smoldering fires according to EN 54.

INTRODUCTION

The assessment of visibility in the context of performance-based fire safety designs generally relies on highly simplified simulation models based on the work of Jin [Jin, 1970]. Assuming spatially homogeneous smoke characteristics, visibility is considered a local phenomenon that can be derived from the corresponding smoke density and luminosity of exit signs. Furthermore, applicants oftentimes apply software defaults for key variables, such as combustion parameters, smoke characteristics or the wavelength of light. Adding up these uncertainties results in low reliability of the of the corresponding estimations. Even the validation of such models by dedicated experimental investigations reveals substantial difficulties. Various studies listed in [McGrattan, 2022] indicate, that smoke concentrations computed with FDS may be overestimated by a factor of up to five. One potential source of uncertainty is considered to be poor scalability of parameters like soot yield Y_s or the mass specific extinction coefficient K_m that contribute directly to the light extinction coefficient σ. Both are usually obtained from bench scale experiments, by means of optical or gravimetric measurements. Acquiring such data from real scale fires at spatial and temporal resolution is therefore inevitable to reliably model light attenuation by

fire smoke. Considering visibility is typically the first variable to exceed a critical threshold in performance-based designs, this becomes even more important.

Determining the soot yield Y_s as well as the corresponding smoke mass density ρ_s from light extinction measurements requires the knowledge of the mass specific extinction coefficient K_m [Mulholland, 1998]. The underlying correlation can be expressed by Beer-Lambert's law.

$$T = \frac{I}{I_0} = \exp(-\sigma \cdot l) = \exp(-K_m \cdot \rho_s \cdot l) \quad (1)$$

Transmission T denotes the fractional obscuration of a light beam with initial intensity I_0 to a value I when passing through a homogeneous medium, here smoke, over a path length l. Since K_m depends on the wavelength, equation (1) is only valid for monochromatic light. A value of $K_m = 8.700\ m^2 kg^{-1}$ for light at $\lambda = 633\ nm$ is commonly referenced as default for flaming combustion in fire models such as FDS. It depicts the mean value from the analysis of seven studies, involving 29 fuels from well-ventilated flaming fires [Mulholland, 2002]. K_m was determined by combined optical measurements of transmittance along with a gravimetric sampling of soot. It can be considered almost fuel-independent for dark smoke particulates, having an absorbing effect predominant over light scattering [Patterson, 1991]. The assumption is valid if the particles are mostly spherical and significantly smaller than the wavelength of the light [Mulholland, 1998]. An empirical correlation of the mass-specific extinction coefficient increasing at lower wavelengths λ was established by Widmann by means of literature research [Widmann, 2003].

$$K_m = 4.8081 \cdot \lambda^{-1.0088} \quad (2)$$

Equation (2) will subsequently be referred to provide comparability of measurement methods operating at different wavelengths.

This paper presents a series of experiments conducted to investigate smoke characteristics in real-scale fires. Comprehensive data is acquired on smoke opacity using the well-established MIREX [CERBERUS, 1991] measurement system as well as a novel photometric approach. The latter allows a spatially and temporally resolved computation of extinction coefficients by deducing the luminosity of LEDs from image data. Furthermore, a continuous analysis of the particle size distribution was performed using the Electrical Low Pressure Impactor (ELPI+). The results will be used in particular to examine homogeneity of the smoke layering.

Finally, temperatures and extinction coefficients obtained from the experiments are used to evaluate a simple FDS simulation model. Potential uncertainties and errors in both the experimental setup and the model are discussed.

EXPERIMENTAL SETUP

Based on previous investigations, smoke characteristics of different test fires in style of EN 54 were analyzed in the current experiments. The focus of the recent study is on the TF 5 n-heptane pool fire as well as the TF 2 wood smoldering fire (see Figure 1). The pool fire is remotely ignited, while the dried wooden sticks are merely pyrolyzed by being heated on a plate.

The adjusted height of the laboratory ceiling was lower than usual (4 m) during the fire tests. This was necessary to allow quick access to the particle measurement equipment without having to move the ceiling after each test. To comply with the framework conditions of EN 54 as far as possible, the amount of material was also reduced from typically 650 g to 500 g n-heptane.

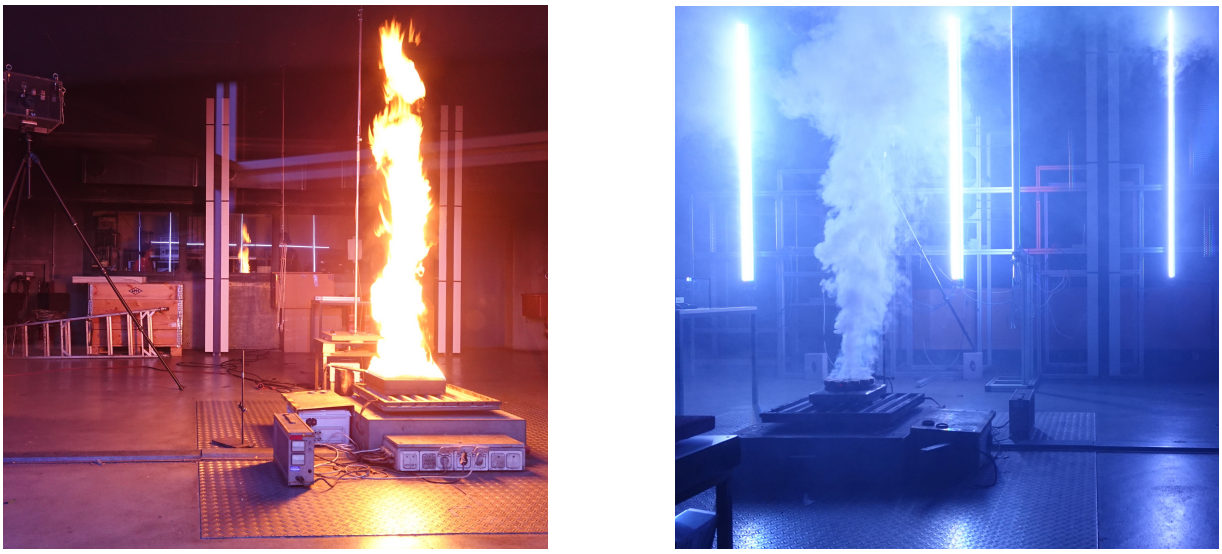

Figure 1: Test fires in style of the EN 54 standard. The TF 5 n-heptane pool fire produces black soot particles, while TF 2 wood smoldering fire generates mostly white smoke.

The experimental setup was similar to that described in [Arnold, 2020], but with an enhanced design and extended measurement technique. The Heinz Luck fire detection laboratory at the University of Duisburg Essen in which the experiments were performed has dimensions of 8.90 m x 10.50 m at a height of 3.37 m (see Figure 2). On a supporting frame structure, a total of six vertical aluminum columns with RGB LED strips adhesively attached were mounted. In varying setups, the individual strips were each operated as white light or single color components. White light here means the red, green and blue LEDs are simultaneously turned on. Using multiple DSLR cameras facing the LED setup, continuous image series are captured during the experiments. This allows to deduce a time series of the transmission values along the line of sight of the cameras to the individual light sources. The applied inverse modelling approach described in [Arnold, 2020] allows computing spatially and temporally resolved values of the extinction coefficients. The model is subject to the assumption of homogeneous smoke layers with a constant thickness, each characterized by a single extinction coefficient. Knowing the relative coordinates of the cameras and the individual LEDs, the spatial discretization allows calculating the path lengths of light beams within the individual layers along the camera's line of sight. Three MIREX devices, serving as reference measurement, are located near the center LED strip at heights of 1.60 m, 2.30 m, and 3.37 m. A detailed description of the measured quantities is provided in the following section.

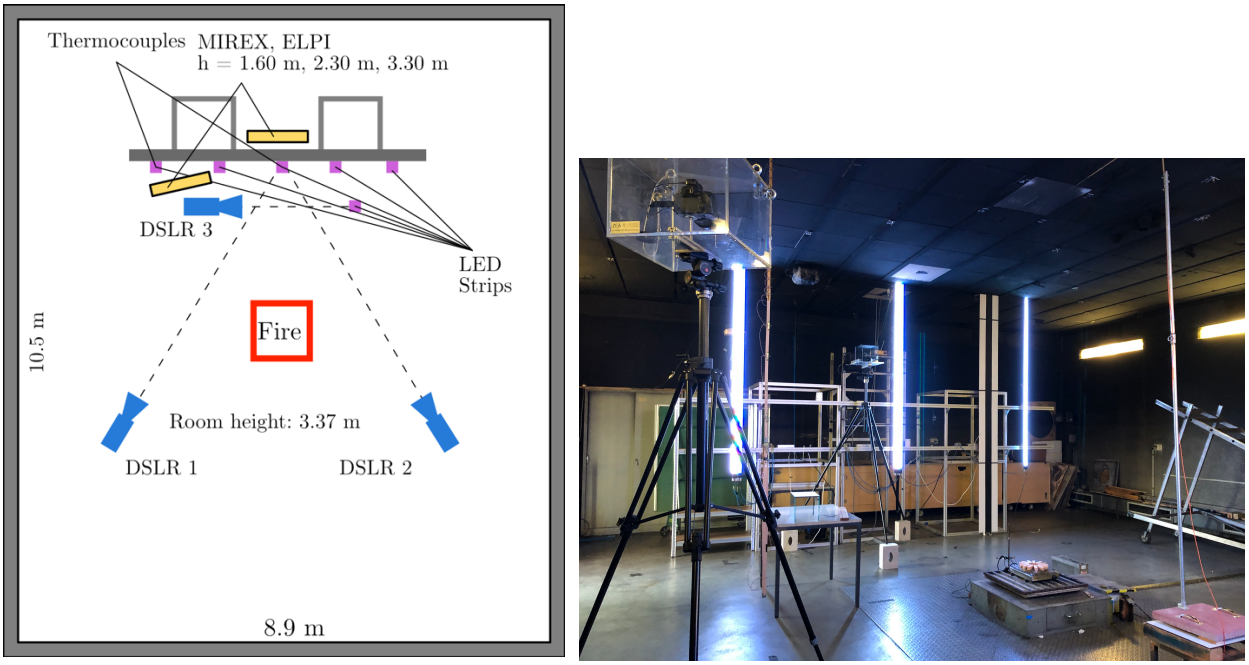

Figure 2: Floor plan and image of the experimental setup within the Heinz Luck Fire Detection Laboratory

Data acquisition is conducted over a period of 30 minutes in each experiment, beginning about one minute before the start of burning or smoldering. The TF 5 fuel (500 g n-heptane) is completely consumed approximately 220 s after the ignition. The laboratory ventilation is turned on 420 s after the fire extinguishes. Smoke formation in the case of the TF 2 is visible roughly 120 s after heating is started, but with a high level of uncertainty. The ventilation system is therefore activated 560 s after the start of the heating phase.

DATA ACQUISITION

Mass Loss

Mass loss is continuously recorded by a balance underneath the fuel tray. This allows to calculate the heat release rate (HRR) of the pool fire by means of the effective heat of combustion of 44.6 MJ kg^{-1} [Babrauskas, 2016]. The HRR reaches a maximum of about 150 kW after 150 s. As part of this study, the TF-2 fire has not yet been evaluated in this regard.

Light obscuration

Two independent approaches have been applied in the experiments to determine the light extinction coefficient due to obscuration by fire smoke. The well-established MIREX device measures light transmission in the infrared regime at a peak wavelength of $\lambda_{\mathrm{MIREX}} = 890$ nm. The total measurement distance between the light source and detector is 2 m passing a reflector. Furthermore, a photometric approach called LEDSA (LED Smoke Analysis) was applied, which is based on a continuous measurement of LED's luminosity. To make the results comparable with the MIREX measurements, the individual color components of the LEDs were spectrally analyzed. Peak wavelengths are given by $\lambda_{\mathrm{red}} = 630$ nm, $\lambda_{green} = 510$ nm and $\lambda_{\mathrm{blue}} = 462$ nm.

The luminosity intensity I of an individual LED is defined as the sum of all pixel values within a surrounding image section (here 20 x 20 pixels). Image series were captured using conventional

consumer DSLR cameras like Canon EOS 70D and 80D. I is normalized to the mean value of ten images, taken before the experiment.

To linearly measure changes in luminosity, the camera's internal post-processing must be avoided. Therefore, only uncompressed RAW images are utilized for the analysis, providing an unbiased interpretation of the camera's sensor data. Common DSLR camera sensors are covered with a spectrally sensitive color filter array according to a particular mosaic pattern (Bayer filter) of which each element only samples a single color. This allows to separate the individual color channels by the respective pixel positions (see Figure 3).

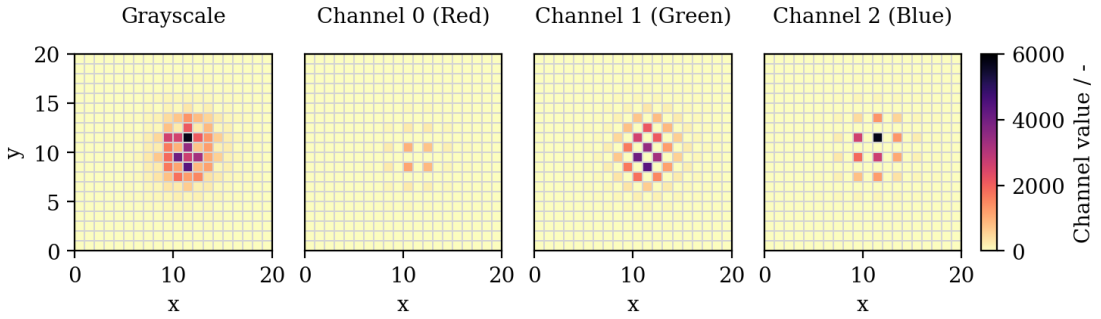

Figure 3: Grayscale image section (20 x 20 pixel) of a single LED and RGB components according to the Bayer filter pattern of the camera sensor

In order to convert the matrix of sensor readings $S(x, y)$ into a grayscale image with pixels $P(x, y)$, the individual elements must be mapped to a fixed dynamic range [Rotjberg, 2017]. A 14-bit resolution of the original signal allows capturing even small changes in the observed transmittance. Linearization is done by scaling between the ground noise B and the saturation level W of the sensor. Subsequently, those fractions are converted to integer values in the target tonal bit range b.

$$P(x, y) = (S(x, y) - B) \cdot \frac{2^{b-1}}{W - B} \tag{3}$$

A simple qualification of the method was conducted by measuring transmission on a single red LED close to the middle MIREX. To allow a quantitative comparison, the extinction coefficient was linearly scaled according to equation (2) using the ratio of the peak wavelengths of the LED and MIREX. Figure 4 shows the resulting extinction coefficient σ comparing both measurement methods, based on a one-meter path length. A camera and LED strip were placed next to the middle MIREX in order to cover a similar field of detection.

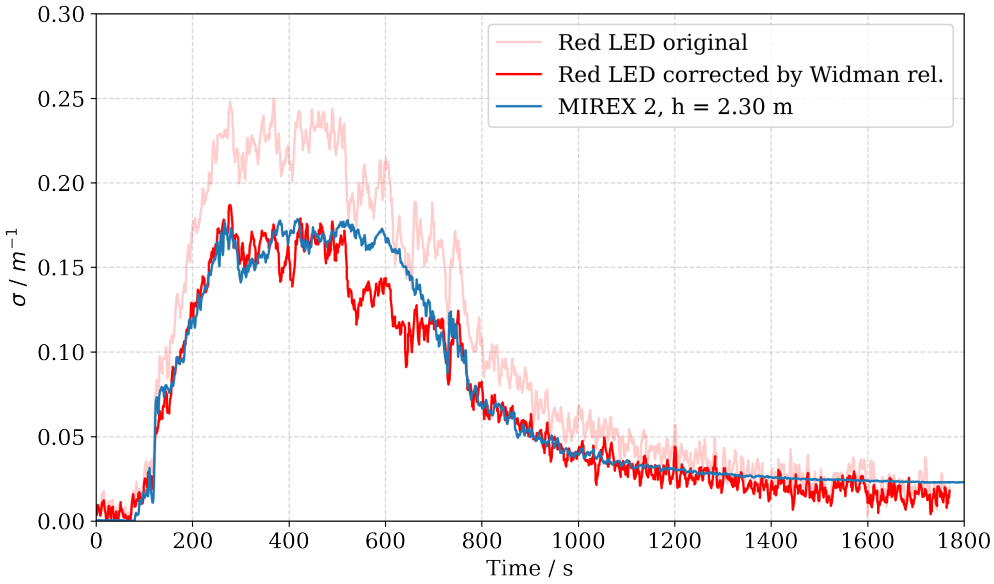

Figure 4: Extinction coefficient according to LEDSA and MIREX, taken on a 1 m path. The LEDSA measurements were scaled by equation (2) according to the wavelength of the MIREX.

Both methods show good agreement, especially in the burning period and after the ventilation is turned on. Significant deviations between 500 s and 700 s cannot be attributed to a particular cause. However, possible reasons for this may be intrinsic to the measurement techniques and to the local deviations in the sampling points.

Temperature

Thermal exposure of the LEDs due to convective heat transfer and radiation from the fire could pose a significant error on the measured luminosity intensity. An exponential loss of the emitted intensity with increasing temperature is reported in [Schubert, 2006]. It varies with the type of semiconductor material used and hence with the LED color. In order to quantify or correct the uncertainties due to thermal exposure, the surface temperature of the LEDs was measured by wire thermocouples. Furthermore, gas temperature was measured by jacket thermocouples in a shaded area 10 cm behind the aluminum columns (see Figure 5). This data is used in particular to assess the homogeneity of the smoke stratification. Moreover, it provides an important quantity for the validation of comparative simulations by CFD models. Both measurements were taken at different heights on the center column and one of the outer columns.

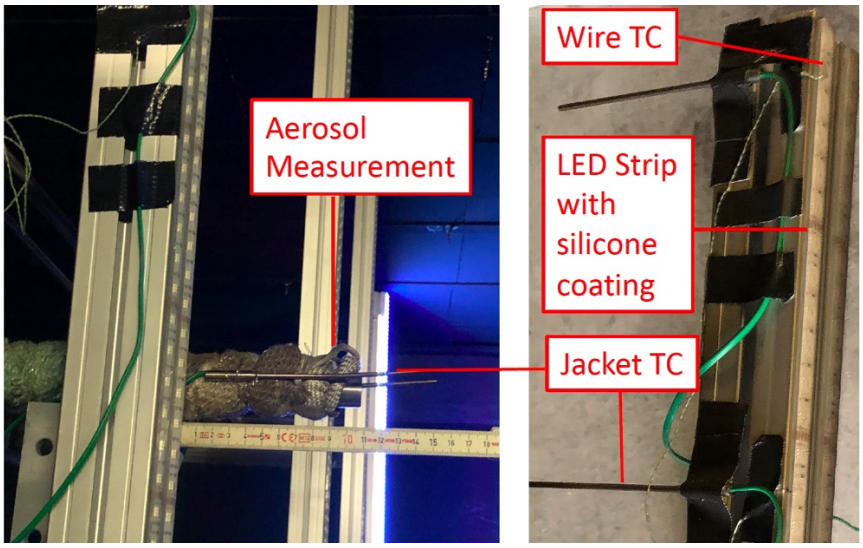

Figure 5: Temperature measurement at the aluminum columns. Wire thermocouples are attached to the LEDs below the thermally insulating silicone coating. Jacket thermocouples are used to measure the gas temperature 10 cm behind the columns. This area is shielded from direct heat radiation by the fire.

Particle Size

Local real-time measurements of particle size distribution were performed during the experiments using an ELPI+ device. The data was acquired to obtain insights into the initial smoke characteristics as well as aerosol aging processes due to agglomeration. Smoke is aspirated through a preheated extractor of adjustable length. When entering the device, the particles are first charged to a known positive state. Depending on their aerodynamic diameter they are size classified within a low-pressure cascade. The particles are collected in different impactor stages where they produce a current that is proportional to the respective number concentration [Dekati, 2011]. Here, the spectral range extends from 6 nm to 10 µm in a total of 14 size bins. To draw conclusions about the correlation of particle size and light transmission, the extractions were taken in close distance to the MIREX devices. Measurements were each taken at a single location that was varied over the course of several experiments.

RESULTS

Repeatability of transmittance measurements

The MIREX measurement results indicate good reproducibility of all TF 5 experiments (see Figure 6). The burning period is characterized by forced convection due to high plume temperatures. Hence, smoke spread is primarily driven by the thermal dynamics of the fire. Once the fire is extinguished and the buoyancy diminishes, environmental conditions tend to have a higher effect on the flow field within the compartment. From the temporal progression of the extinction coefficient at the different heights, the descent of the smoke layer becomes evident. Between 200 s and 400 s, the decrease of the upper MIREX readings is accompanied by an increase of the lower ones.

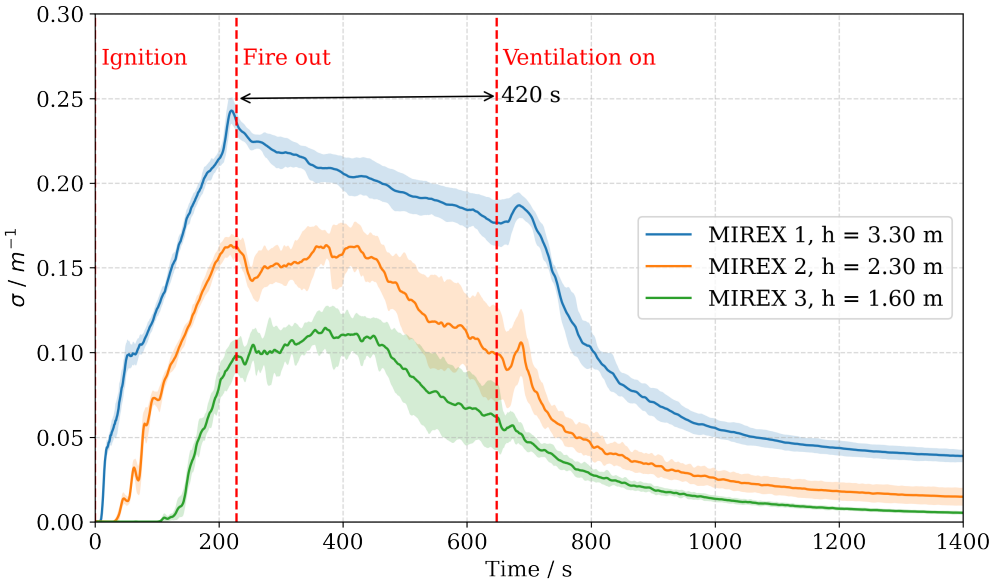

Figure 6: Mean value and standard deviation of the extinction coefficient of 17 TF 5 experiments performed at different days. Measurements were taken by three MIREX devices at heights 1.6 m, 2.3 m and 3.37 m above the floor level.

In contrast, the TF 2 experiments (see Figure 7) show several uncertainties about repeatability. When compared to the n-heptane fuel, the charred wooden blocks are more inhomogeneous in terms of material properties and moisture. The pyrolysis process is accompanied by negligible heat emission, so that the resulting smoke is driven by low buoyancy. Furthermore, it is difficult to temporally align the experimental runs since the initial formation of smoke generation is highly ambiguous.

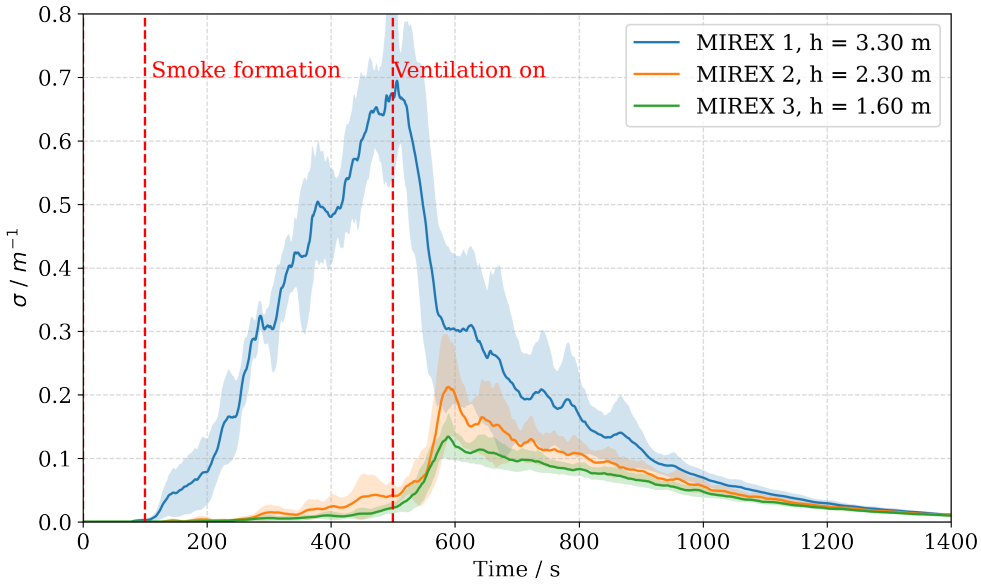

Figure 7: Mean value and standard deviation of the extinction coefficient of nine TF 2 experiments performed at different days. Measurements were taken by three MIREX devices at heights 1.6 m, 2.3 m and 3.37 m above the floor level.

The deposition of smoke particles differs significantly in both test fires. While dark residue was clearly visible on setup and instruments after the TF 5 experiments, there was little evidence of this on the TF 2 fires. This becomes particularly apparent in TF 5 transmission readings, not returning to the initial level once the smoke has been completely cleared from the laboratory. A similar, although slightly weaker, effect shows up in the LEDSA results (see Figure 4).

Particle size distribution

At this point, the evaluation of the particle size distribution only serves the qualitative spatially resolved comparison of two measurement series. Figure 8 depicts the temporal evolution of the size distribution for two TF 5 experiments. The smoke was extracted underneath the ceiling at a distance of 1.70 m respectively 3.00 m from the center of the fire plume axis. The spectra of both measurements show a similar shape, corresponding to a log normal distribution. Considering the uncertainty of the measurement device and the individual discrepancies between two experiments, this supports the hypothesis of homogeneous smoke characteristics at a horizontal level.

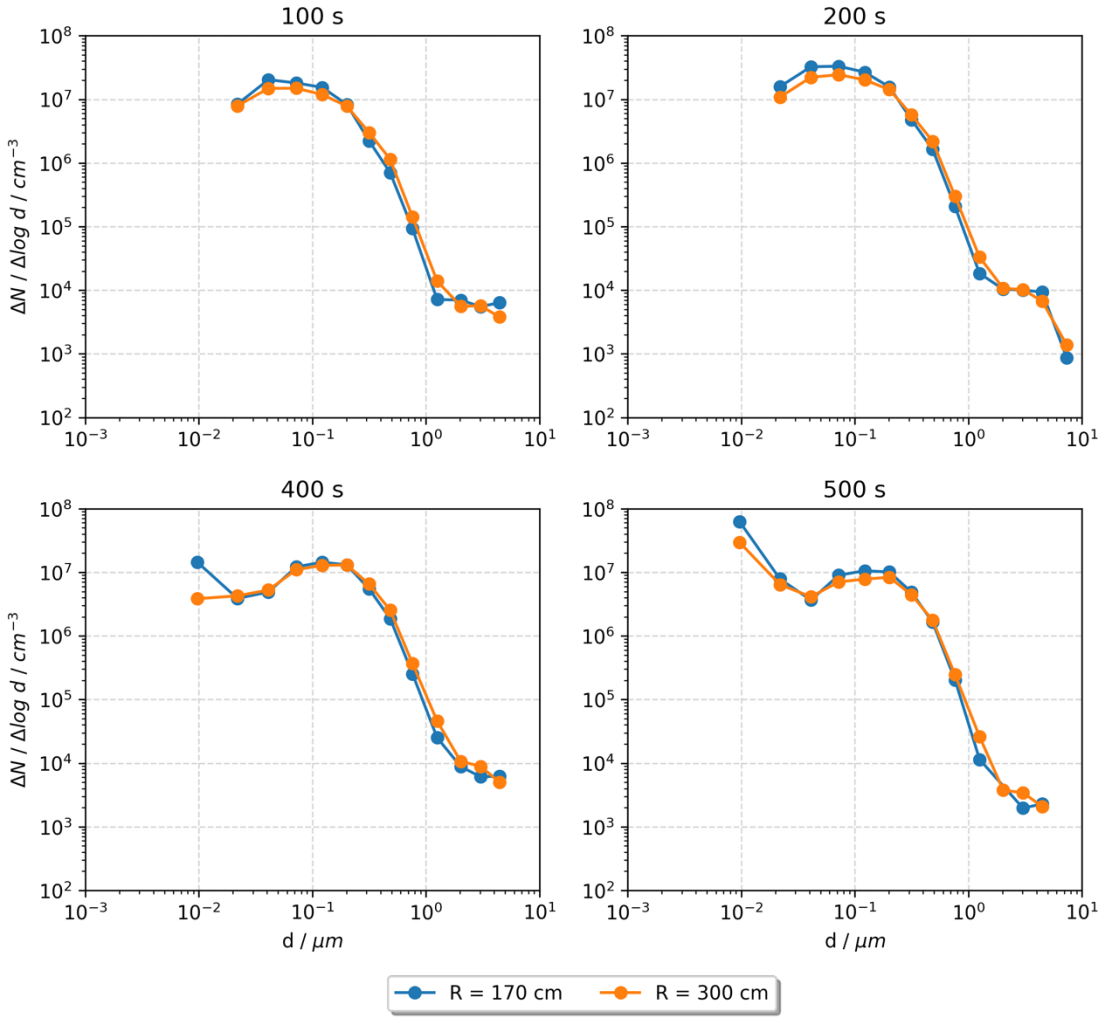

Figure 8: Particle size distribution from the ELPI+ measurements of two TF 5 experiments at different times after the ignition. The extractor was located 15 cm below the ceiling at a horizontal distance of 1.70 m and 3.00 m from the center of the fire source.

It can be seen that the spectrum shifts towards larger particle diameters with time, which can be essentially attributed to the agglomeration effects. This particularly applies to the time after the fire goes out and no new particles emerge (400 s and 500 s).

FDS MODEL VALIDATION

Boundary conditions and model parameters

An FDS simulation was set up according to the actual laboratory geometry, taking into account the thermophysical boundary conditions of the building components. Here, only the TF 5 n-heptane pool fire will be addressed, as it is the simplest to model. The HRR was defined according to the mass loss rate recorded in the experiments. The mass-specific extinction coefficient was chosen to be the default FDS value of $K_m = 8.700\ \mathrm{m^2 kg^{-1}}$. Furthermore, the soot yield was set to a commonly adopted value of $Y_S = 0.037$ for n-heptane fires [Tewarson, 2002]. Apart from that, the simulation largely matches the boundary conditions of the model as described in [Arnold, 2021].

FDS results vs experiment

A grid sensitivity study indicates the relevant quantities, i.e., gas temperature and smoke density, converge at the chosen cell size of 8 cm. The qualitative analysis of these data supports the hypothesis of a homogeneous horizontal smoke stratification. Particularly for the burning period, a distinct layering emerges, as can be seen at 100 s and 200 s in Figure 9. After the fire is extinguished, the smoke gases gradually turn more diffuse due to the lack of buoyancy.

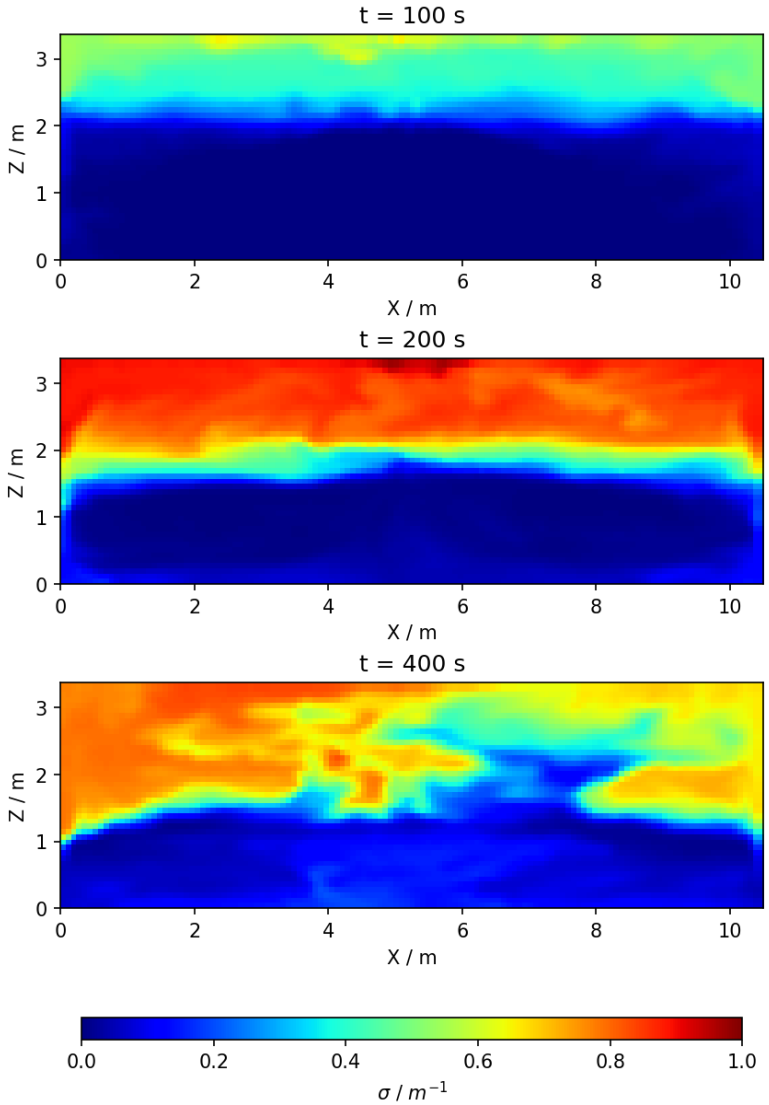

Figure 9: FDS slice file showing a cross-section view in the plane of the LED setup. It depicts the spatial resolution of the extinction coefficient at different times.

The extinction coefficients computed with FDS generally exceed the measurements of both techniques to a significant extent. Comparing the equivalent simulation data with the upper MIREX readings reveals the latter to be regularly overestimated by factor 4.5 across the burning period. Similar discrepancy among experimental studies and FDS simulations is reported in [Gottuk, 2008]. A major cause for this is attributed to the adopted soot yield, since commonly applied literature values are usually obtained from small scale fires in bench-scale calorimetry apparatus. Furthermore, the neglected soot loss resulting from deposition on enclosing components is considered to be a decisive cause for the model to overpredict the measured smoke concentrations. Floyd et al. examined these effects by modeling deposition and gravitational settling along with aerosol aging processes [Floyd, 2014]. They conclude that FDS predictions get close to the experimental data, especially when smoke particles are assumed to be relatively large.

To allow a qualitative comparison of the MIREX and LEDSA data with the simulation results, the latter were linearly scaled by a factor of 1/4.5 according to observed discrepancy. Furthermore, all

values were mapped to the wavelength $\lambda = 632\ nm$ according to equation (2). Figure 10 shows the measured and computed values of the extinction coefficient by height at different times.

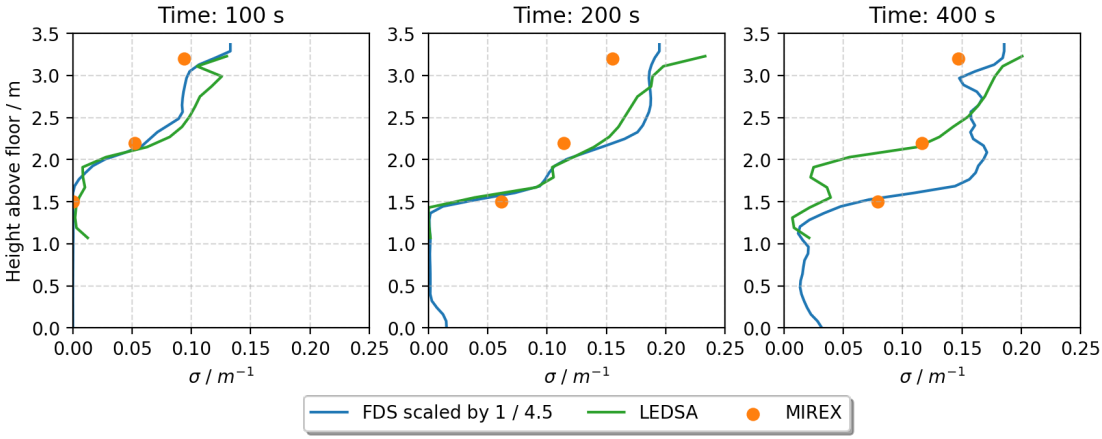

Figure 10: Height profile of extinction coefficients from LEDSA, MIREX and FDS at different times. The FDS results have been linearly scale by the factor of 1/4.5 according to the discrepancy of simulation and measurement data.

The similarly shaped profile of the smoke layering at 100 s and 200 s supports the hypothesis of the simulation model to correctly represent the fluid dynamics phenomena. Hence, it suggests that, according to equation (1), the deviation results from the chosen input parameters of K_M and or Y_s.

The focus of the temperature analysis here is on the jacket thermocouples behind the aluminum bars. These are primarily relevant for the comparison with the simulation results. For simplification, the gas temperature is employed as the reference quantity in FDS, since the radiant heat impact on the thermocouples is likely to be negligible. However, uncertainty arises from the inertia of the thermocouples, as can be seen in Figure 11. At the time of the maximum measured gas temperature, both experimental and FDS results are in good agreement. Considerable deviations can be observed before and after this period as a result of delayed warming and cooling.

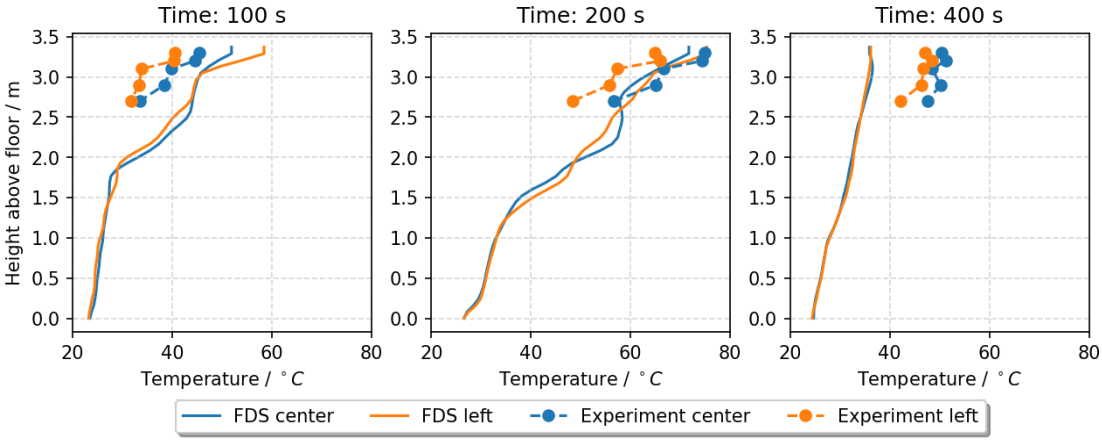

Figure 11: Height profile of ambient temperatures from FDS simulation and experimental measurements at different times

LEDs close to the ceiling heat up by a maximum of 58°C due to thermal exposure during the experiments. The lower heating of the LEDs against the ambient temperature may essentially result

from the thermal insulating coating. To minimize the error on the measured intensities, all LEDs were run until they reached an absolute steady-state temperature of about 40°C prior to the experiments. This results in a maximum delta of 18°C compared to the operating temperature of the LEDs. According to [Schubert, 2006] this may pose a 10 % drop in the emitted intensity at least for red LEDs of type AlGaInP. The error on the green and blue LEDs is likely to be significantly lower.

CONCLUSION AND OUTLOOK

Validation of a simplified FDS model reveals that the computed extinction coefficient may significantly overestimate the outcomes obtained from experimental measurements. However, the results indicate that the discrepancies result more from the chosen input parameters than from the model itself. In terms of performance-based assessments, this might cause highly conservative predictions of visibility in case of fire. Consequences of that involve unreasonably high expenses for constructional and technical measures.

The experimental results can be assumed reliable as they show a high repeatability with good agreement of two independent measurement techniques. Certain simplifications of the simulation model may be partially accounted for the deviations from the experimental results. This includes, for example, disregarding deposition and agglomeration of the soot particles. However, this does not explain high deviations even in the early burning phase, when only few variations in the size distribution can be observed. The major variables affecting the computed extinction coefficient are the soot yield and the mass-specific extinction coefficient. Both are usually obtained from bench-scale experiments and may not be necessarily applicable for modelling real-scale fires. Comparing the extinction coefficient in temporal and spatial resolution shows an almost linear deviation between simulation and experiment. This supports the assumption that the error may essentially be attributed to these input quantities. At the same time, it implies that the fluid dynamics and transport processes related to smoke particles are well represented by FDS, at least while the stated aerosol effects have a negligible influence. Further simulations will take these mechanisms into account using the available FDS submodels. Here, the conducted particle measurements will also serve for validation purposes. However, the existing models in FDS still face some substantial limitations with respect to the computation of the light extinction coefficient. For instance, for the agglomeration kernel, the assumption is made that the particle number density is uniform throughout the compartment. This underpredicts agglomeration, especially in the flow field of the plume and ceiling jet. Moreover, the mass-specific extinction coefficient varies with the shape and size distribution of the particles. Both effects cannot be accounted for within FDS.

Investigating the spatial and temporal dynamics of the soot particle size will be an essential aspect of future work. The available data set already allows to analyze aging processes of different aerosols at multiple heights within the smoke layering. Furthermore, the LEDSA data may be used to draw conclusions on smoke characteristics by applying approaches like described in [Flecknoe-Brown, 2015] and [Cashdollar, 1979]. These methods involve experimental measurements of light transmission at multiple wavelengths along with theoretical calculations based on Mie scattering theory in order to estimate the particle mean diameter of aerosols.

REFERENCES

McGrattan, K., Hostikka, S., Floyd, J., McDermott, R., & Vanella, M. (2022). Fire Dynamics Simulator Technical Reference Guide Volume 3: Validation – Version 6.7.8 (tech. rep.).

Arnold, L., Belt, A., Schulze, T., & Mughal, A. W. (2021). Experimental and Numerical Investigation of Visibility in Compartment Fires. AUBE 21.

Arnold, L., Belt, A., Schultze, T., & Sichma, L. (2020). Spatiotemporal measurement of light extinction coefficients in compartment fires. Fire and Materials.

Babrauskas , V. (2016). Chapter: Heat Release Rate. SFPE Handbook of Fire Protection Engineering (5th). Springer.

Cashdollar, K. L., Lee, C. K., & Singer, J. M. (1979). Three-wavelength light transmission technique to measure smoke particle size and concentration. Applied Optics, 18 (11), 1763.

CERBERUS LTD (1991). Extinction measuring equipment MIREX. Technical description.

Dekati Ltd. (2011). ELPI+ User Manual.

European Committee for Standardization. (2002). EN 54 - Fire detection and fire alarm systems, part 7: smoke detectors point detectors using scattered light, transmitted light or ionization.

Flecknoe-Brown, K. W., & Hees, P. v. (2015). Obtaining Additional Smoke Characteristics Using Multi-Wavelength Light Transmission Measurements. 14th International Conference and Exhibition on Fire and Materials 2015.

Floyd, J., Overholt, K., & Ezekoye, O. (2014). Soot Deposition and Gravitational Settling Modeling and the Impact of Particle Size and Agglomeration. 11, 376–388.

Gottuk, D., Mealy, C., & Floyd, J. (2008). Smoke Transport and FDS Validation. Fire Safety Science, 9, 129–140.

Jin, T. (1970). Visibility through Fire Smoke (I). Bulletin of Japan Association for Fire Science and Engineering, 19 (2), 1–8.

Mulholland, G. W., & Choi, M. Y. (1998). Measurement of the mass specific extinction coefficient for acetylene and ethene smoke using the large agglomerate optics facility. Symposium (International) on Combustion, 27 (1), 1515–1522.

Mulholland, G. W., & Croarkin, C. (2000). Specific extinction coefficient of flame generated smoke. Fire and Materials, 24 (5), 227–230.

Patterson, E., Duckworth, R., Wyman, C., Powell, E., & Gooch, J. (1991). Measurements of the optical properties of the smoke emissions from plastics, hydrocarbons, and other urban fuels for nuclear winter studies. Atmospheric Environment. Part A. General Topics, 25 (11), 2539–2552.

Rotjberg, P. (2017). Processing RAW images in Python (tech. rep.).

Schubert, E. F. (2006). Light-Emitting Diodes (Vol. Second edition). Cambridge University Press.

Tewarson, A. (2002). Chapter: H Generation of Heat and Chemical Compounds in Fires. SFPE Handbook of Fire Protection Engineering (3rd). Springer.

Widmann, J. F. (2003). Evaluation of the planck mean absorption coefficients for radiation transport through smoke. Combustion Science and Technology, 175 (12), 2299–2308.